Magnetism and superconductivity in $M_5Rh_4Ge_{10}$ (M=Gd, Tb, Dy, Ho, Er, Tm, Lu, and Y)

N. G. Patil and S. Ramakrishnan
Tata Institute of Fundamental Research, Mumbai-400005, India
(Received 12 January 1998; revised manuscript received 9 September 1998)

Low-temperature resistivity, magnetization and heat-capacity studies are reported for the isostructural $M_5Rh_4Ge_{10}$ (M=Gd, Tb, Dy, Ho, Er, Tm, Lu, and Y) series. Some of the compounds (M=Gd, Tb, Er, and Tm) show multiple magnetic transitions below 15 K while others (M=Dy and Ho) exhibit only a single magnetic transition. The four magnetic transitions observed for $Gd_5Rh_4Ge_{10}$ and $Tb_5Rh_4Ge_{10}$ are unusual in that the one at the highest temperature is a second-order phase transition while the other three are first-order transitions probably involving moment reorientations. An anisotropic exchange interaction is proposed as the cause of the multiple transitions. Of the nonmagnetic compounds, $Lu_5Rh_4Ge_{10}$ shows superconductivity below 2.4 K whereas $Y_5Rh_4Ge_{10}$ remains normal down to 1.7 K. The results are compared with those of the previously investigated $M_5Ir_4Si_{10}$ series. [S0163-1829(99)01613-6]

I. INTRODUCTION

Ternary rare-earth silicides and germanides form in a rich variety of crystal structures.[1,2] Some of them incorporate traditionally magnetic 3d elements such as Co, Fe, and Ni while retaining their superconducting properties. It turns out that in these compounds, the 3d atoms have no magnetic moment on them. However, they participate in building up a high density of states at the Fermi level which is responsible for the superconductivity. In particular, some rare-earth compounds with the tetragonal $Sc_5Co_4Si_{10}$ ($P4/mbm$) prototype structure[3] show the coexistence of magnetism and superconductivity with possible charge-density-wave ordering at higher temperatures.[3–16] One of the interesting features of this structure is the absence of direct transition-transition metal contacts. The transition-metal atoms are connected to each other either through a rare-earth or Si/Ge atom. This is in marked contrast to the cluster type superconducting compounds such as, MMo_6S_8 (Ref. 17) and MRh_4B_4,[18] which have been studied in great detail. Earlier studies[19–20] showed that it was possible to form the $M_5Rh_4Ge_{10}$ series with heavy rare-earth elements (and also with Y). Since some of the compounds belonging to the $M_5Ir_4Si_{10}$ series[4,8] exhibit unusual superconducting and magnetic properties, it was anticipated that similar properties would be exhibited by the $M_5Rh_4Ge_{10}$ family. With this in view, as a part of our detailed study of this series, we report resistivity (2–300 K), magnetization (2–300 K) and heat-capacity (2–35 K) measurements for $M_5Rh_4Ge_{10}$ (M=Gd, Tb, Dy, Ho, Er, Tm, Lu, and Y). Our results for the $M_5Rh_4Ge_{10}$ series will be compared with those from previous investigations of the $M_5Ir_4Si_{10}$ series. The results are divided into three groupings (A, B, and C) to facilitate comparison among compounds with nonmagnetic ground state (A), compounds that have single magnetic transitions (B) and those which exhibit multiple transitions (C).

II. EXPERIMENTAL DETAILS

Samples of the $M_5Rh_4Ge_{10}$ (M=Gd, Tb, Dy, Ho, Er, Tm, Lu, and Y) system were made by melting the individual constituents (taken in stoichiometric proportions) in an arc furnace under high-purity argon atmosphere. The purity of the rare-earth metals and also that of Rh was 99.9% whereas the purity of Ge was 99.999%. The alloy buttons were remelted five to six times to ensure proper mixing. The samples were annealed under high vacuum (10^{-6} torr) at 900°C for a week. The x-ray powder-diffraction pattern of the samples did not show the presence of any impurity phases and the lattice constants a and c are in agreement with those reported in a previous study.[19] The unit cell of the tetragonal $M_5Rh_4Ge_{10}$ structure is shown in Fig. 1. The Rh and Ge atoms form planar nets of pentagons and hexagons which are stacked parallel to the basal plane and connected along c axis via Rh-Ge-Rh zigzag chains. The pentagon and hexagon layers are separated by layers of rare-earth atoms. The Rh-Ge and Ge-Ge distances are short indicating strong covalent interactions. The values of a and c are given in Table I with

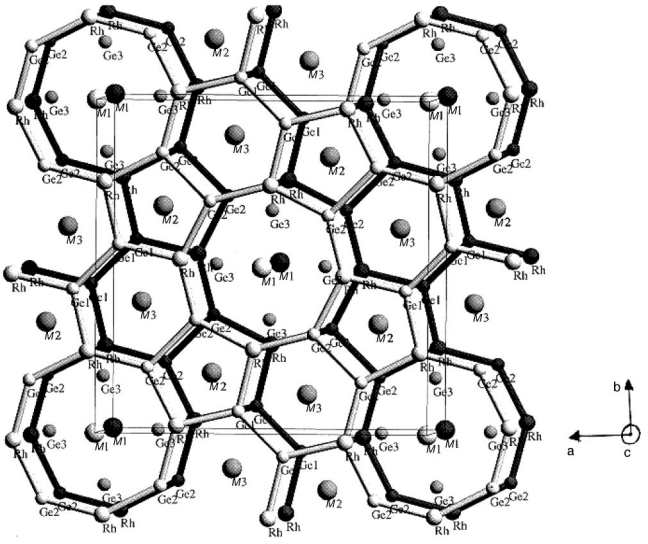

FIG. 1. Unit cell of the tetragonal $M_5Rh_4Ge_{10}$ (M = Gd, Tb, Dy, Ho, Er, Tm, Lu, and Y) structure. There are 38 atoms in the unit cell and the interesting feature is the absence of direct Rh-Rh bonds. The rare-earth atom has three sites with different symmetries.

TABLE I. Structural properties of $M_5Rh_4Ge_{10}$.

Sample	a(Å)	c(Å)	V(Å^3)
$Gd_5Rh_4Ge_{10}$	12.984±0.005	4.296±0.005	239.7
$Tb_5Rh_4Ge_{10}$	12.954±0.005	4.285±0.005	237.8
$Dy_5Rh_4Ge_{10}$	12.932±0.005	4.266±0.005	235.3
$Ho_5Rh_4Ge_{10}$	12.911±0.005	4.252±0.005	233.5
$Er_5Rh_4Ge_{10}$	12.880±0.005	4.238±0.005	231.4
$Tm_5Rh_4Ge_{10}$	12.856±0.005	4.228±0.005	229.8
$Lu_5Rh_4Ge_{10}$	12.827±0.005	4.209±0.005	227.2

respective error. The temperature dependence of susceptibility (χ) was measured using the Faraday method in a field of 4 kOe in the temperature range from 3 to 300 K. Isothermal magnetization studies in some of the samples have been carried out using a commercial superconducting quantum interference device magnetometer (MPMS of Quantum Design Inc., USA) at various temperatures. The resistivity was measured using a four-probe dc technique with contacts made using silver paint on a cylindrical sample of 2 mm diameter and 10 mm length. The temperature was measured using a calibrated Si diode (Lake Shore Inc., USA) sensor. The sample voltage was measured using a nanovoltmeter (model 182, Keithley, USA) with a current of 10 mA using a 20 ppm stable (model 220, Keithley, USA) current source. All the data were collected using an IBM compatible PC/AT via IEEE-488 interface. The heat capacity in zero field between 2 and 35 K was measured using an automated adiabatic heat-pulse method. A calibrated germanium resistance thermometer (Lake Shore Inc, USA) was used as the temperature sensor in this range.

III. RESULTS

A. Normal nad superconducting state properties of $Lu_5Rh_4Ge_{10}$ and $Y_5Rh_4Ge_{10}$

1. Magnetic susceptibility studies

The dc magnetic susceptibility (χ) of $Lu_5Rh_4Ge_{10}$ in its normal state ranges from 3.2×10^{-4} emu/mol at 250 K to 1.6×10^{-3} emu/mol at 10 K. Such a weak temperature dependence of χ could arise due to two reasons. One of them could be the presence of magnetic rare-earth impurities in ''pure'' Lu (99.9%) and we need at least 900 ppm of Gd to account for the observed temperature dependence of χ. Although Gd is a common impurity in Lu we believe that such a large Gd concentration is unlikely. The second reason could be the temperature variation of the density of states at the Fermi level which results in a temperature-dependent Pauli spin susceptibility as seen in some of the A-15 compounds.[21] Knight-shift measurements (^{175}Lu-NMR) would be useful to resolve this issue.

2. Resistivity studies

The temperature dependence of the resistivity (ρ) of $Lu_5Rh_4Ge_{10}$ and $Y_5Rh_4Ge_{10}$ is shown in Fig. 2. The inset shows that the low-temperature ρ data for $Lu_5Rh_4Ge_{10}$ undergo a sharp jump at 2.4 K which corresponds to the superconducting transition temperature (T_c) of this sample. This

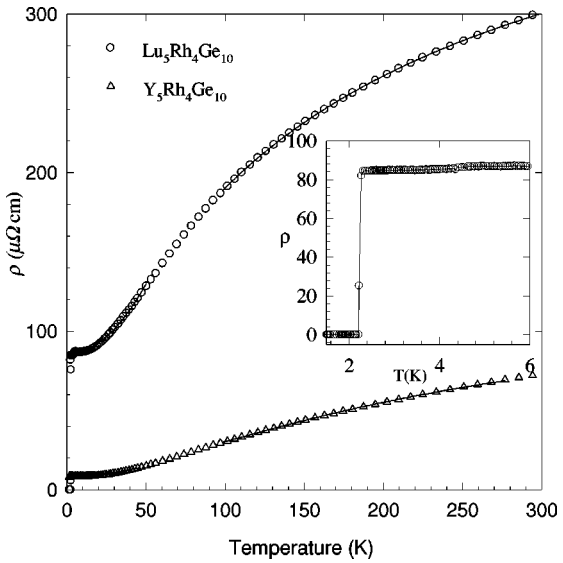

FIG. 2. Temperature dependence of resistivity (ρ) of $Lu_5Rh_4Ge_{10}$ and $Y_5Rh_4Ge_{10}$ from 2 to 300 K. The low-temperature ρ data for $Lu_5Rh_4Ge_{10}$ (inset) reveal the superconducting transition at 2.4 K with a width of 0.1 K. The solid lines are theoretical fits.

is in agreement with the T_c value obtained from χ data. The transition width (ΔT_c) of 0.1 K is much smaller than the previously reported value of 0.6 K.[19] In the normal state (5 K$<T<$25 K), the low-temperature dependence of ρ could be described by the power law

$$\rho=\rho_0+aT^n, \tag{1}$$

and the fitted values of ρ_0, a, and n are given in Table II. For both specimens the optimum values of n is found to be 3 which agrees with Wilson's s-d scattering model for $T<\theta_D/10$.

At high temperatures (100 K$<T<$300 K), the ρ data significantly deviate from linear temperature dependence as has seen in many other compounds where the ρ value is high. This occurs because the mean free path becomes short, of the order of few atomic spacings. When that happens, the scattering cross section will no longer be linear in the scattering perturbation. Since the dominant temperature-dependent scattering mechanism is the electron-phonon interaction here, the ρ will no longer be proportional to the mean-square atomic displacement, which is proportional to T for a harmonic potential. Instead, the resistance will rise less rapidly than linearly in T and will show negative curvature ($d^2\rho/dT^2<0$). This behavior is also seen in previous studies on silicides and germanides.[12,14]

One of the models which describe the $\rho(T)$ of these compounds is known as the parallel resistor model.[22] In this model the expression of $\rho(T)$ is given by

$$\frac{1}{\rho(T)}=\frac{1}{\rho_1(T)}+\frac{1}{\rho_{\max}}, \tag{2}$$

where $\rho_{\max}$ is the saturation resistivity which is independent of temperature and $\rho_1(T)$ is the ideal temperature-dependent resistivity. Further, the ideal resistivity is given by the following expression:

TABLE II. Parameters obtained from low and high-temperature resistivity fits in $M_5Rh_4Ge_{10}$. T_0 (T_N or T_c) is the ordering temperature except for $Y_5Rh_4Ge_{10}$ which does not order down to 1.7 K.

Sample	Low-temperature fit ($T_0<T<30$ K)			High-temperature fit (100 K$<T<$300 K)			
	ρ_0 $\mu\Omega$ cm	a $n\Omega$ cm/K^n	n	ρ_{max} $\mu\Omega$ cm	ρ_0 $\mu\Omega$ cm	C	θ_D K
$Gd_5Rh_4Ge_{10}$	31.2	4.88	2	280	51	63	413
$Tb_5Rh_4Ge_{10}$	33.0	1.05	2	465	49	500	277
$Dy_5Rh_4Ge_{10}$	22.4	6.17	2	348	31	324	272
$Ho_5Rh_4Ge_{10}$	16.6	5.9	2	201	40	553	477
$Er_5Rh_4Ge_{10}$	37.3	17.9	2	593	52	708	239
$Tm_5Rh_4Ge_{10}$	23.5	22.5	2	507	59	464	214
$Lu_5Rh_4Ge_{10}$	87.4	0.56	3	445	60	713	123
$Y_5Rh_4Ge_{10}$	8.22	0.42	3	167	19	412	500

$$\rho_1(T)=\rho_0+C_1\left(\frac{T}{\theta_D}\right)^3\int_0^{\theta_D/T}\frac{x^3dx}{[1-\exp(-x)][\exp(x)-1]}, \tag{3}$$

where ρ_0 is the residual resistivity and the second term is due to phonon-assisted electron scattering similar to the s-d scattering in transition metal compounds. θ_D is the Debye temperature and C_1 is a numerical constant. Equation (2) can be derived if we assume that the electron mean free path l is replaced by $l+a$ (a being an average interatomic spacing). Such an assumption is reasonable, since infinitely strong scattering can only reduce the electron mean free path to a. Chakraborty and Allen[23] have made a detailed investigation of the effect of strong electron-phonon scattering within the framework of the Boltzmann transport equation. They find that the interband scattering opens up new *nonclassical channels* which account for the parallel resistor model. The values of the various parameters obtained from the high-temperature fit to the model are listed in Table II.

3. Heat-capacity studies

The temperature dependence of the heat capacity (C_p) from 2 to 35 K for $Lu_5Rh_4Ge_{10}$ and $Y_5Rh_4Ge_{10}$ is shown in Fig. 3. The inset shows the low-temperature C_p data for $Lu_5Rh_4Ge_{10}$. The jump in C_p at 2.4 K ($\Delta C_p=30$ mJ/mol K) shows bulk superconducting ordering in agreement with the above resistivity measurement. The temperature dependence of C_p was fitted to the expression

$$C_p=\gamma T+\beta T^3, \tag{4}$$

where γ is due to the electronic contribution and β is due to the lattice contribution. In the temperature range from 10 to 20 K this yielded 2.9 mJ/Lu mol K^2 and 2.95 mJ/mol K^4 and 1.6 mJ/ Y mol K^2 and 1.8 mJ/mol K^4 for γ and β in $Lu_5Rh_4Ge_{10}$ and $Y_5Rh_4Ge_{10}$, respectively. For $Lu_5Rh_4Ge_{10}$ the value of the ratio $\Delta C_p/\gamma T_c$ is 0.9 which is significantly reduced from the BCS value of 1.43. Low values of $\Delta C_p/\gamma T_c$ may arise from an extrinsic effect such as magnetic impurities or due to a two-band contribution similar to the case of the $Lu_2Fe_3Si_5$ series.[24] Using the relation

$$\theta_D=\left(\frac{12\ \pi^4\ Nr\ k_B}{5\beta}\right)^{1/3}, \tag{5}$$

where N is Avogadro's number, r is the total number of atoms per formula unit, and k_B is Boltzmann's constant, we estimate $\theta_D=232$ K for $Lu_5Rh_4Ge_{10}$ and $\theta_D=273$ K for $Y_5Rh_4Ge_{10}$.

B. MAGNETIC PROPERTIES OF $M_5Rh_4Ge_{10}$ (M=Dy, Ho, Er, Tm)

1. Magnetic susceptibility studies

The temperature dependence of the inverse dc magnetic susceptibility (χ^{-1}) of $M_5Rh_4Ge_{10}$ (M=Dy, Ho, Er, and Tm) samples is shown in Fig. 4. The inset shows the low-temperature susceptibility behavior of Dy, Ho, and Er samples. This inset indicates that Dy^{3+}, Ho^{3+}, and Er^{3+} spins order antiferromagnetically below 6, 5, and 5 K, respectively. The high-temperature susceptibility (100 K$<T<$300 K) is fitted to a modified Curie-Weiss expression which is given by

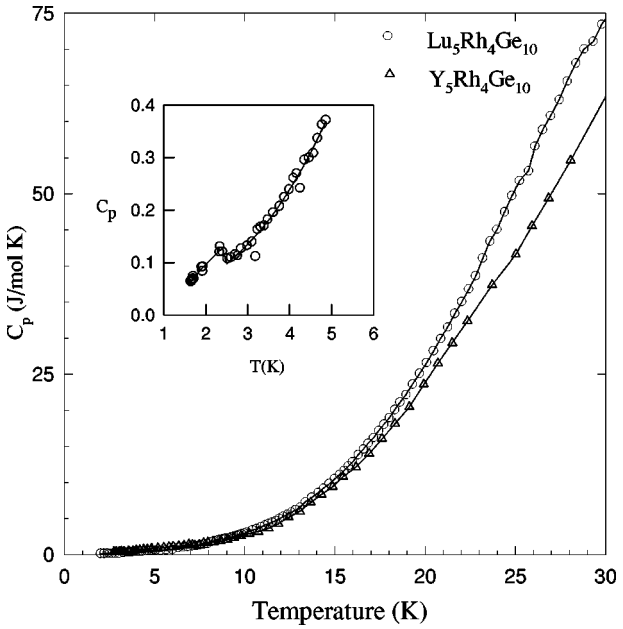

FIG. 3. Plot of C_p vs T of $Lu_5Rh_4Ge_{10}$ and $Y_5Rh_4Ge_{10}$ from 1.9 to 30 K. The inset shows the same plot from 1.5 to 6 K to elucidate the jump at 2.4 K ($\Delta C_p=30$ mJ/mol K) which demonstrates the bulk superconductivity.

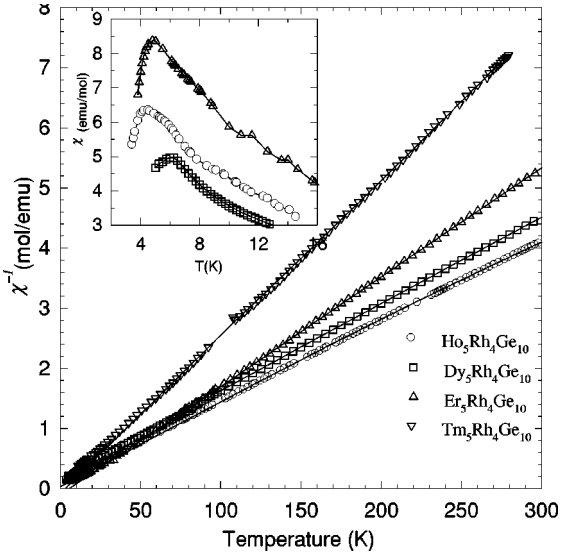

FIG. 4. Variation of inverse dc susceptibility ($1/\chi$) of $M_5Rh_4Ge_{10}$ (M=Ho, Dy, Er, and Tm) from 3 to 300 K in a field of 4 kOe. The inset shows the χ behavior from 3 to 16 K. The solid line is a fit to the Curie-Weiss relation (see text for details).

$$\chi = \chi_0 + \frac{C}{(T-\theta_p)}, \tag{6}$$

where C is the Curie constant which can be written in terms of the effective moment as

$$C(\text{emu K/mol}) = \frac{\mu_{\text{eff}}^2 x}{8}. \tag{7}$$

Here, x is the concentration of M ions ($x=5$ for $M_5Rh_4Ge_{10}$), and μ_{eff} is given in terms of μ_B. The main contributions to the temperature independent χ_0 are the diamagnetic susceptibility (which arises due to the presence of ion cores) and the susceptibility of the conduction electrons. The fitted values of χ_0, μ_{eff}, and θ_p are included in Table III. In each case, the effective moment is less than 5% smaller than the ideal, free-ion value, μ_{th} (which is also included in Table III for the purpose of comparison). Although all four specimens were observed to order antiferromagnetically at low temperature, the fitted θ_p values are negative only for $Dy_5Rh_4Ge_{10}$ and $Tm_5Rh_4Ge_{10}$ which could be due to the splitting of energy levels due to the crystal-electric field (CEF). However, only below 100 K do the χ data of all samples show a deviation from the Curie-Weiss plot which could be ascribed to the presence of crystal-field contributions. Figure 5 shows the isothermal magnetization data of $Dy_5Rh_4Ge_{10}$ at temperatures of 5, 10, and 25 K. The nonlinear behavior in M vs H at 5 K agrees with the suggestion of antiferromagnetic ordering of Dy^{3+} spins. At higher temperature ($T=15$ K$>T_N$), one observes linear behavior in magnetization which characterizes the paramagnetic state.

TABLE III. Parameters obtained from the high-temperature susceptibility fit to the Curie-Weiss relation in $M_5Rh_4Ge_{10}$. μ_{th} is the theoretical value.

Sample	χ_0	μ_{eff}	μ_{th}	θ_p
$Gd_5Rh_4Ge_{10}$	0.84	8.11	7.9	−25.95
$Tb_5Rh_4Ge_{10}$	−9.48	10.42	9.7	−24.5
$Dy_5Rh_4Ge_{10}$	2.4	10.45	10.63	−11.6
$Ho_5Rh_4Ge_{10}$	2.4	10.07	10.4	2.5
$Er_5Rh_4Ge_{10}$	2.5	9.29	9.59	8.4
$Tm_5Rh_4Ge_{10}$	−7.1	8.15	8.5	−3.5
$Lu_5Rh_4Ge_{10}$	0.17			
$Y_5Rh_4Ge_{10}$	0.29			

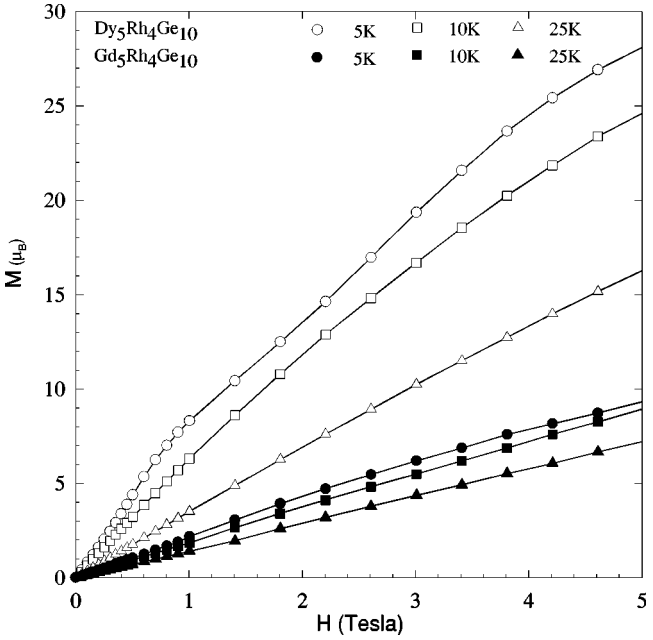

FIG. 5. Isothermal magnetization (M) vs magnetic field (H) at 5, 10, and 25 K of $Dy_5Rh_4Ge_{10}$ and $Gd_5Rh_4Ge_{10}$. The nonlinearity in M vs H at 5 K agrees with the notion of antiferromagnetic ordering of Dy^{3+} spins and Gd^{3+} spins whereas the linear behavior of M on H at 25 K signifies that the sample is in the paramagnetic state at this temperature.

2. Resistivity studies

The temperature dependence of the resistivity (ρ) of $M_5Rh_4Ge_{10}$ (M=Dy, Ho, Er, and Tm) is shown in Fig. 6. The inset shows a drop in resistivity at 5.6, 6, 5.5, and 6.5 K which represent the antiferromagnetic ordering temperature (T_N) of $M_5Rh_4Ge_{10}$ for M=Dy, Ho, Er, and Tm, respectively. These are close to the T_N values obtained from the χ data. In the low-temperature resistivity data of $Tm_5Rh_4Ge_{10}$, a slope change is observed at 5 K as well as at 6.5 K. Hence, there is probably a second transition in this sample. In the paramagnetic region (10 K$<T<$30 K), the low-temperature dependence of ρ of all of these samples could be described by the power law given by Eq. (1) and the fitted values of the parameters ρ_0, a, and n are given in Table II. The optimum value of n is 2 suggesting that spin fluctuations dominate the electron scattering at these temperatures. At high temperatures, the ρ behavior is similar to that observed in $Lu_5Rh_4Ge_{10}$ and the data could be fitted to the parallel resistor model. Estimated Debye temperature and other fitted parameters are also given in Table II.

3. Heat-capacity studies

The temperature dependence of C_p from 3 to 35 K (3 to 20 K for $Tm_5Rh_4Ge_{10}$) is shown in Fig. 7. The antiferromag-

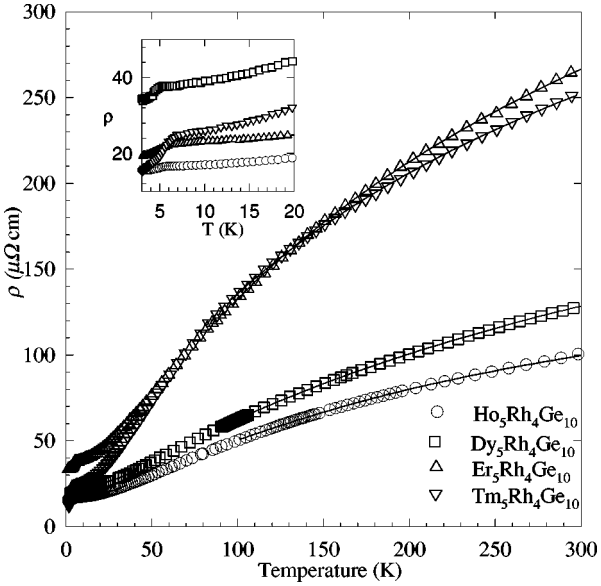

FIG. 6. Temperature dependence of resistivity (ρ) of $M_5Rh_4Ge_{10}$ (M=Ho, Dy, Er, and Tm) from 3 to 300 K. The inset shows the low-temperature behavior of ρ from 2 to 20 K. The solid line is a fit to the parallel resistor model (see text).

netic transition is observed as a sharp maximum at T_N =6.2, 6.3, 5.6, and 6.9 K for M=Dy, Ho, Er, and Tm, respectively. The origin of a small shoulder at 5 K for $Dy_5Rh_4Ge_{10}$ is not yet known. Further sharp transitions are observed below T_N at 4.2 K for $Er_5Rh_4Ge_{10}$ (see inset of Fig. 7) and at 6 K for $Tm_5Rh_4Ge_{10}$. These most likely correspond to first-order spin reorientation transitions. For example, in the case of Er it could be an incommensurate to commensurate transition such as the one observed in $Er_2Fe_3Si_5$.[25] These transition temperatures are summarized in Table IV. Included in Table V are the total entropies per unit rare-earth ion at both the Néel temperature and at 35 K. In each case, the entropy at 35 K is considerably less than the

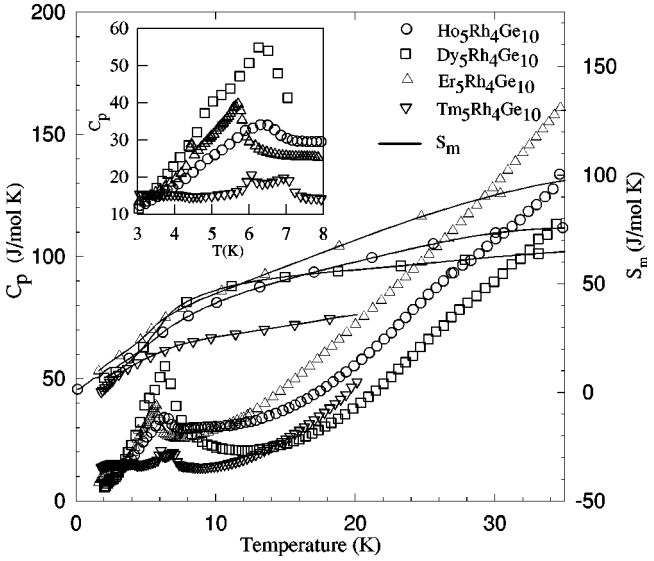

FIG. 7. Plot of C_p vs T of $M_5Rh_4Ge_{10}$ (M=Ho, Dy, Er, and Tm) The calculated values of entropy S_m are also given in the same figure, from 3 to 35 K.

TABLE IV. Transition temperatures from different measurement techniques. Transition temperatures refer to antiferromagnetic ordering except when they are explicitly stated otherwise.

Sample	Transition temperatures (K) Resistivity	Susceptibility	Heat capacity
$Gd_5Rh_4Ge_{10}$	14,11,9,6.5	14,8.5,6.5	14,11,9,6.5
$Tb_5Rh_4Ge_{10}$	11.5,5,3.5,2.5	11.5[a]	11.5,4.5,3.8,3
$Dy_5Rh_4Ge_{10}$	5.6	6	6.2
$Ho_5Rh_4Ge_{10}$	4.5	6	6.3
$Er_5Rh_4Ge_{10}$	5.5	5	5.6,4.2
$Tm_5Rh_4Ge_{10}$	6.5		6,6.9
$Lu_5Rh_4Ge_{10}$	2.4[b]		2.4[b]

[a]Other three transitions are not clearly discernible from χ data.
[b]Superconducting transition.

value of $R\ln(2J+1)$ expected for a free ion (also included in Table V for ease of comparison). This confirms that CEF's are important. The total entropy at T_N matches closely with that of doublet ground state (possibly a doublet or a two-singlet ground state in case of the non-Kramer Ho^{3+} and Tm^{3+} ions.)

C. Magnetic properties of $Tb_5Rh_4Ge_{10}$ and $Gd_5Rh_4Ge_{10}$

1. Magnetic susceptibility studies

The temperature dependence of the inverse dc magnetic susceptibility (χ^{-1}) of $Tb_5Rh_4Ge_{10}$ and $Gd_5Rh_4Ge_{10}$ from 3 to 300 K is shown in Fig. 8. The inset shows the susceptibility behavior at low temperatures. Antiferromagnetic ordering of Tb^{3+} spins is clearly seen at 11.5 K whereas a similar transition for $Gd_5Rh_4Ge_{10}$ occurs at 14 K. In addition to this metamagnetic transitions are observed at 8.5 and 6.5 K for $Gd_5Rh_4Ge_{10}$. In both samples high-temperature susceptibility (100 K$<T<$300 K) is fitted to Eq. (6). The estimated effective moments are comparable to their respective free ion moment. The negative value of θ_p is in agreement with observed antiferromagnetic ordering of Tb^{3+} and Gd^{3+} spins. The values of the parameters are listed in Table III for comparison. Figure 5 shows the isothermal magnetization data of $Gd_5Rh_4Ge_{10}$ at various temperatures from 5 to 25 K. The nonlinear behavior in M vs H at 5 K agrees with the notion of antiferromagnetic ordering of Gd^{3+} spins. This nonlinear

TABLE V. Parameters obtained from the specific-heat measurement in $M_5Rh_4Ge_{10}$. Entropy values are estimated for unit trivalent rare-earth ion and R is the gas constant.

Sample	$T_N(K)$* K	$S(T_N)/R$	J	$\ln(2J+1)$	$S(35\text{ K})/R$
$Gd_5Rh_4Ge_{10}$	14	1.68	$\frac{7}{2}$	2.079	1.998
$Tb_5Rh_4Ge_{10}$	11.5	0.92	6	2.565	1.3
$Dy_5Rh_4Ge_{10}$	6.2	0.75	$\frac{1}{5}$	2.773	1.59
$Ho_5Rh_4Ge_{10}$	6.3	0.72	8	2.833	1.73
$Er_5Rh_4Ge_{10}$	5.6	0.77	$\frac{15}{2}$	2.773	2.41
$Tm_5Rh_4Ge_{10}$	6.9	0.77	6	2.56	1.2[a]

[a]Entropy estimates at 20 K.

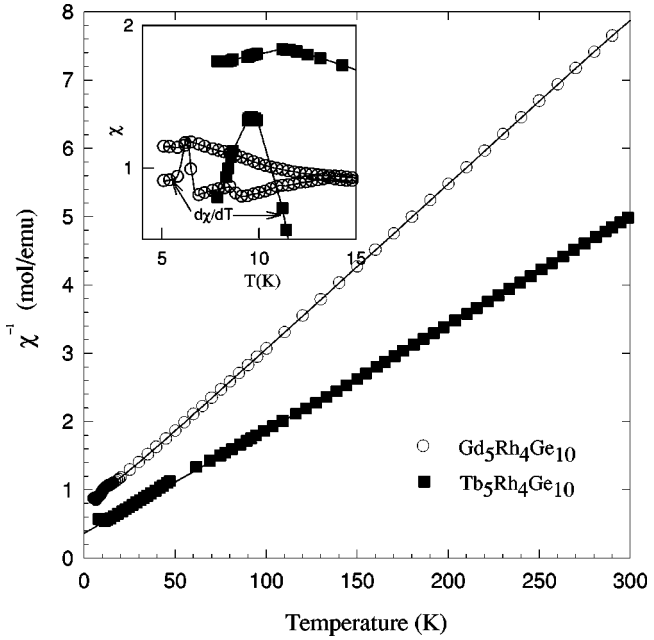

FIG. 8. Variation of inverse dc susceptibility ($1/\chi$) of $Tb_5Rh_4Ge_{10}$ and $Gd_5Rh_4Ge_{10}$ from 3 to 300 K in a field of 4 kOe. The inset shows temperature variation of both χ and $d\chi/dT$ from 6 to 20 K. The solid line is a fit to the Curie-Weiss relation (see text for details).

behavior persists up to 10 K albeit with a much smaller value. At higher temperature ($T=25$ K$>T_N$), one observes the usual linear behavior in magnetization which characterizes the paramagnetic state.

2. Resistivity studies

The temperature dependence of the resistivity (ρ) of $Tb_5Rh_4Ge_{10}$ and $Gd_5Rh_4Ge_{10}$ is shown in Fig. 9. The inset shows the low-temperature ρ data on an expanded scale. The ρ data for $Tb_5Rh_4Ge_{10}$ show a sudden drop in resistivity at 11.5 K which is in agreement with antiferromagnetic ordering observed via dc susceptibility measurements. The ρ data show kinks at 5, 3.5, and 2.5 K, which could be due to multiple transitions involving Tb^{3+} reorientations. The ρ data for $Gd_5Rh_4Ge_{10}$ also show a cusp in resistivity at 14 K representing antiferromagnetic ordering of Gd^{3+}. We have also observed a change of slopes in ρ data (by computing $d\rho/dT$, not shown in the figure) at 11, 9, and 6.5 K, respectively, representing other transitions which have been seen in χ data. In the paramagnetic region ($10\text{ K}<T<30$ K), the temperature dependence of ρ could be fitted to the power law given by Eq. (1). The optimum value of n is found to be 2 and the values of ρ_0 and a are given in Table II. This value of n once again suggests the dominance of spin fluctuations in the paramagnetic state at low temperatures. At high temperatures, the ρ behavior is similar to that observed in other compounds of this series. Resistivity data could be fitted to the parallel resistor model. The values of the fitted parameters are also given in Table II.

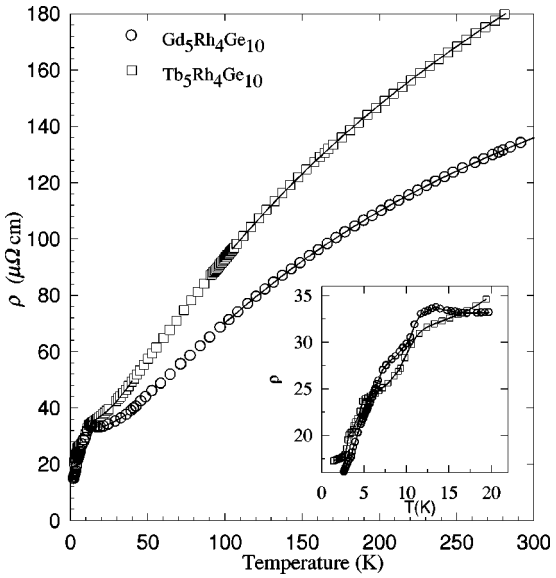

FIG. 9. Temperature dependence of resistivity (ρ) of $Tb_5Rh_4Ge_{10}$ and $Gd_5Rh_4Ge_{10}$ from 2 to 300 K. The inset shows the low-temperature behavior of ρ from 2 to 16 K. The sharp change in ρ implies multiple transitions in these samples. The solid line is a fit to the parallel resistor model (see text).

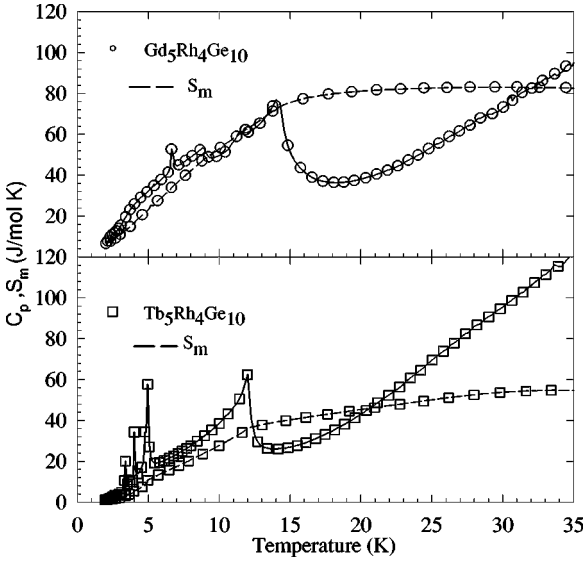

FIG. 10. Plot of C_p vs T of $Tb_5Rh_4Ge_{10}$ and $Gd_5Rh_4Ge_{10}$ from 2 to 35 K. Four magnetic transitions of Tb^{3+} spins can be seen at 12, 5, 4, and 3.5 K. The sharp peaks below the second-order transition at 12 K suggest first-order phase transitions at lower temperatures. Quadruple magnetic transitions of Gd^{3+} spins are also observed at 14, 11, 8, and 6 K. The sharp peaks below the second-order transition at 14 K suggest first-order phase transitions at lower temperatures. The calculated values of entropy S_m are also given in the same figure.

3. Heat-capacity studies

The temperature dependence of C_p from 1.8 to 35 K of $Tb_5Rh_4Ge_{10}$ and $Gd_5Rh_4Ge_{10}$ is shown in Fig. 10. The large jump at 12.0 K ($\Delta C=35$ J/mol K) in C_p of $Tb_5Rh_4Ge_{10}$ shows the bulk nature of magnetic ordering which has been seen in susceptibility and resistivity data as well. We also observed sharp transitions at 5, 4, and 3.5 K in C_p data which are in accordance with ρ data. The sharpness suggests that these transitions are probably first order and could be due to spin reorientation below the second-order antiferro-

magnetic ordering at 13 K. Entropy at 35 K is found to be 10.82 J/Tb mol K which is much less than expected value of $R\ln(2J+1)$ and this indicates the presence of crystal-field contributions. In $Gd_5Rh_4Ge_{10}$, large jump at 14 K ($\Delta C = 40$ J/mol K) shows the bulk nature of magnetic ordering as seen in susceptibility and resistivity data. However, further transitions are seen at 11.5, 9, and 6.5 K in the C_p data which are in accordance with ρ and χ data. The origin of these first-order transitions may be due to spin reorientations below the first antiferromagnetic transition at 13 K. Entropy at 35 K is found to be 16.6 J/Gd mol K which is close to the value of $R\ln(2J+1)$.

IV. DISCUSSION

From Table II, most of the samples have resistivity values typical of rare-earth compounds at low-temperatures except $Lu_5Rh_4Ge_{10}$. This is due to the inherent disorder in the structure which arises because of the smallness of the size of Lu^{3+} ion. The low-temperature resistivity of the rare-earth compounds containing magnetic elements show T^2 dependence suggesting the dominance of spin fluctuations. Although we could fit the high-temperature dependence of ρ to the parallel resistor model (see Table II) successfully, the θ_D values obtained from such fits do not agree with those obtained from heat-capacity data for at least two nonmagnetic compounds ($Y_5Rh_4Ge_{10}$ and $Lu_5Rh_4Ge_{10}$). One of the causes could be due to anharmonic contribution which is not considered in the parallel resistor model. The values of $\rho_{\max}$ also vary considerably across the series. Our results show the inapplicability of parallel resistor model to these samples. More investigations are clearly needed here to understand the transport properties of these compounds. We now turn our attention to some of the systematic trends observed in these data. We find single magnetic transition in $Dy_5Rh_4Ge_{10}$ and $Ho_5Rh_4Ge_{10}$ whereas $Er_5Rh_4Ge_{10}$ and $Tm_5Rh_4Ge_{10}$ show double transitions. Four transitions are observed in $Gd_5Rh_4Ge_{10}$ and $Tb_5Rh_4Ge_{10}$. In general, the antiferromagnetic ordering temperatures for a series of isostructural and isoelectronic metals are expected to scale as $(g_J-1)^2\ J(J+1)$ where g_J is the Lande g factor and J is the total angular momentum of the local moment. If the angular momentum is quenched then T_N is expected to scale as $S(S+1)$.

The solid line in Fig. 11 represents the ordering temperatures expected for various compounds based on heavy rare-earth elements of the series $M_5Rh_4Ge_{10}$ normalized to the observed ordering temperature (highest one) of $Gd_5Rh_4Ge_{10}$ since S is a good quantum number in this case. The dashed line is obtained by similar normalization to the observed ordering temperature of $Gd_5Rh_4Ge_{10}$ and gives the ordering temperatures for the case where J is the good quantum number. From Fig. 11, it is evident that the ordering temperatures of the compounds do not follow the de Gennes scaling $(g_J-1)^2\ J(J+1)$. The fact that many of them do not follow the de Gennes[26] scaling implies that the main interaction leading to the magnetic transitions in this series is not the Ruderman-Kittel-Kasuya-Yosida (RKKY) interaction. All compounds containing the magnetic rare-earth elements approximately show an entropy change of $R\ln 2$ at T_N which implies a doublet ground state. Large contributions from the CEF's are evident since the full entropy is not released at 35 K in all

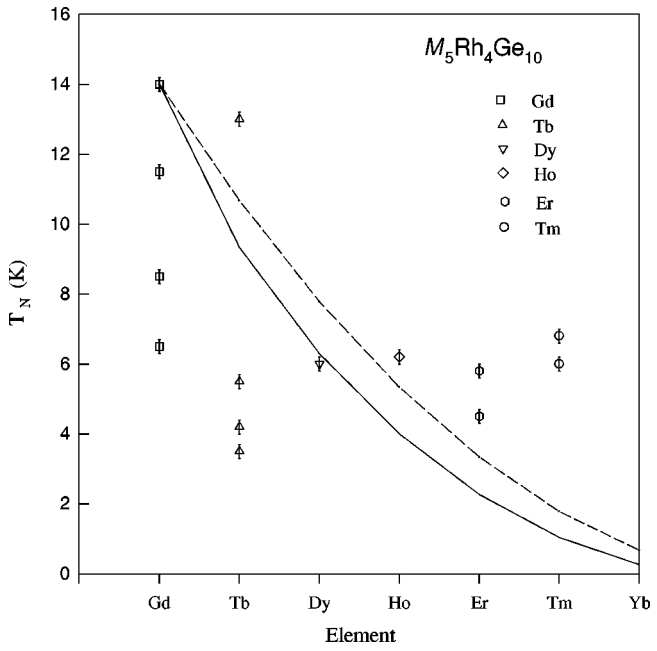

FIG. 11. Plot of the ordering temperatures of the compounds of the series $M_5Rh_4Ge_{10}$ (M=Gd, Tb, Dy, Ho, Er, and Tm). The dashed lines represent the scaling law where only spin quantum number S is used whereas the solid lines are for scaling law using total quantum number J (de Gennes scaling, see text for details).

compounds except in the case of $Gd_5Rh_4Ge_{10}$ where there is no CEF contribution. It is well known that the CEF can enhance or in some cases decrease the magnetic transition temperature[27] and this could, in principle, account for the difference between the observed data and the de Gennes scaling. If we add the CEF terms to the exchange Hamiltonian, one can write an expression for the transition temperature as

$$T_N = \frac{2\ G(g_J-1)^2 \Sigma_{J_z} J_z^2 \exp(-3B_2^o J_z^o/T_N)}{\Sigma_{J_z}[\exp(-3B_2^o J_z^2/T_N)]}, \qquad (8)$$

where G is the exchange constant for the $4f$ atoms and B_2^0 is the crystal-field parameter.[28] Since Gd is an S-state ion, its ordering temperature can be used to fix the value of the exchange constant. However, we find that the calculated values of T_N are lower than the observed values of T_N if one uses the B_2^0 values from our preliminary CEF analysis. Hence, we believe that the main reason for the discrepancy between observed T_N and that found from de Gennes scaling may not be due to CEF's.

Usually one observes at best only two magnetic transitions in Gd-based intermetallic compounds.[29,30] Hence, the observation of four transitions in $Gd_5Rh_4Ge_{10}$ is a unique feature and to the best of our knowledge has not been reported in any Gd-based intermetallic compounds. The sharper fall in C_p at 14 K on the high-temperature side probably implies a usual second-order transition whereas the other three sharp transitions which occur at low temperatures could be due to successive spin-reorientation effects. The slope $(d\chi/dT)$ changes in the magnetization data at these transitions are in agreement with the suggestion of first-order transitions. However, at present, this is only a conjecture

which has to be verified by direct microscopic techniques such as magnetic x-ray scattering and electron-spin resonance. Neutron-scattering measurements are difficult due to high absorption of neutrons by Gd and Rh. In general, as we have stated before, the magnetic ordering temperatures of compounds based on rare-earth elements (especially the compounds containing heavy rare-earth elements) in the same series follow the de Gennes curve implying that the RKKY interaction is the dominant interaction term. However, this is not so in the $M_5Rh_4Ge_{10}$ series. Hence, the magnetic ordering is not entirely due to isotropic exchange (RKKY). One of the interactions which could be dominant here is the anisotropic exchange interaction.[31]

In the case of $4f$ systems, there is a large spin-orbit coupling because the orbital contribution to the magnetic moment is only partially quenched by the crystal field. This means, because of the highly directional nature of the $4f$ orbitals, that the exchange between two f ions may be expected to contain certain anisotropic terms,[32] which depend on the angles between the magnetic moments and the crystallographic axes as well as on the relative angle between the magnetic moment vectors. The presence of such anisotropic interactions have been demonstrated by Birgeneau and others.[33] This anisotropic interaction causes the canting of the local moments only if the total symmetry is the same in the canted as well as the uncanted state. The canting angle is usually of the order of the ratio of the anisotropic to isotropic exchange interaction. Such a theory, in principle, could account for the multiple transitions in systems where $L \neq 0$, such as, $Tb_5Rh_4Ge_{10}$. However, such a theory cannot be used for $Gd_5Rh_4Ge_{10}$ since $L=0$ in this case. Here we must also mention that the situation in $Gd_5Rh_4Ge_{10}$ and $Tb_5Rh_4Ge_{10}$ is quite complicated due to the presence of 10 rare-earth atoms in the unit cell with at least two different site symmetries. Single-crystal studies are useful in this case and efforts to grow them are in progress.

Finally, in the structure of the $M_5Ir_4Si_{10}$ series (as in the case of $M_5Rh_4Ge_{10}$), there are multiple sites for the rare-earth atoms and the minimum distance between any two rare-earth atoms is greater than 5 Å. Moreover, the bond distance between rare earth's in any one of the three sites with the Ir atom is greater than 3 Å. These distances are large enough so that the exchange interaction between the magnetic rare-earth atom and the conduction electrons is weak. That is why the antiferromagnetic ordering temperature in $M_5Ir_4Si_{10}$ is quite low. Although the $M_5Rh_4Ge_{10}$ series is structurally similar to the $M_5Ir_4Si_{10}$ series, it is quite possible that the presence of Rh increases the conduction electron density in $M_5Rh_4Ge_{10}$ as compared to $M_5Ir_4Si_{10}$ which could account for the higher values of their magnetic ordering temperatures. The absence of the charge-density-wave transition in $M_5Rh_4Sn_{10}$ series could be due to their larger unit-cell volume compared to that of the $M_5Ir_4Si_{10}$ series.

V. CONCLUSION

To conclude, we have observed antiferromagnetic ordering in all compounds of the series $M_5Rh_4Ge_{10}$ containing magnetic rare-earth elements below 15 K. Some of them exhibit multiple magnetic transitions which we ascribe to the anisotropic exchange interaction, except for those of $Gd_5Rh_4Ge_{10}$. The nonmagnetic sample $Lu_5Rh_4Ge_{10}$ shows bulk superconductivity at 2.4 K whereas $Y_5Rh_4Ge_{10}$ remains normal down to 1.7 K. The magnetic ordering temperatures of $M_5Rh_4Ge_{10}$ are larger than those of the $M_5Ir_4Si_{10}$ system. The unusual multiple transitions observed in $Gd_5Rh_4Ge_{10}$ and $Tb_5Rh_4Ge_{10}$ deserve further studies, preferably on single crystals.

[1] E. Parthe and B. Chabot, in *Handbook of Physics and Chemistry of Rare Earths*, edited by K.A. Gschneidner, Jr. and L. Eyring (Elsevier Science, North-Holland, Amsterdam, 1984), Vol. 6, pp 113–334.

[2] P. Rogl, in *Handbook of Physics and Chemistry of Rare Earths*, edited by K.A. Gschneidner, Jr. and L. Eyring (Elsevier Science, North-Holland, Amsterdam, 1984), Vol. 7, pp. 1–264.

[3] H.F. Braun K. Yvon, and R. M. Braun, J. Less-Common Met. **100**, 105 (1984).

[4] H.F. Braun, in *Ternary superconductors*, edited by G.K. Shenoy, B.D. Dunlap, and F.Y. Fradin (North-Holland, Amsterdam, 1980), p. 225.

[5] R.N. Shelton, L.S. Hausermann-Berg, P. Klavins, H.D. Yang, M.S. Anderson, and C.A. Swenson, Phys. Rev. B **34**, 4590 (1986).

[6] Po-Jen Chu, B.C. Gerstein, H.D. Yang, and R.N. Shelton, Phys. Rev. B **37**, 1796 (1988).

[7] C.A. Swenson, R.N. Shelton, P. Klavins, and H.D. Yang, Phys. Rev. B **43**, 7668 (1991).

[8] H.D. Yang, P. Klavins, and R.N. Shelton, Phys. Rev. B **43**, 7681 (1991).

[9] K. Ghosh, S. Ramakrishnan, and Girish Chandra, Phys. Rev. B **48**, 4152 (1993).

[10] B. Becker, N. G. Patil, S. Ramakrishnan, A. A. Menovsky, G. J. Nieuwenhuys, and J. A. Mydosh, Phys. Rev. B **59**, 7266 (1999).

[11] S. Ramakrishnan, K. Ghosh, and Girish Chandra, Phys. Rev. B **45**, 10 769 (1992).

[12] S. Ramakrishnan, K. Ghosh, and Girish Chandra, Phys. Rev. B **46**, 2958 (1992).

[13] S. Ramakrishnan, K. Ghosh, Arvind D. Chinchure, Kristian Jonason, V.R. Marathe, and Girish Chandra, Phys. Rev. B **51**, 8398 (1995).

[14] K. Ghosh, S. Ramakrishnan, and Girish Chandra, Phys. Rev. B **48**, 4152 (1993).

[15] K. Ghosh, S. Ramakrishnan, Arvind D. Chinchure, K. Jonason, V.R. Marathe, and Girish Chandra, and S.S. Shah, Phys. Rev. B **51**, 11 656 (1995).

[16] S. Ramakrishnan and K. Ghosh, Physica B **223&224**, 154 (1996).

[17] O. Pena and M. Sergent, Prog. Solid State Chem. **19**, 165 (1989).

[18] Φ. Fisher, in *Ferromagnetic Materials*, edited by K.H.J. Buschow and E.P. Wohlfarth (Elsevier, Holland, 1990), Chap. 6.

[19] G. Venturini, M. Meot-Meyer, E. McRae, J.F. Mareche, and B. Roques, Mater. Res. Bull. **19**, 1647 (1984).

[20] L.S. Hausermann-Berg and R.N. Shelton, Phys. Rev. B **35**, 4673 (1987).

[21] M. Weger and I.B. Goldberg, in *Solid State Physics: Advances in Research and Applications*, edited by H. Ehrenreich, F. Seitz, and D. Turnbull (Academic, New York, 1973), Vol. 28, p. 1.

[22] H. Wiesmann, M. Gurvitch, H. Lutz, A. Ghosh, B. Schwarz, M. Strongin, P.B. Allen, and J.W. Halley, Phys. Rev. Lett. **38**, 782 (1977).
[23] B. Chakraborty and P.B. Allen, Phys. Rev. Lett. **42**, 736 (1979).
[24] C.B. Vining, R.N. Shelton, H.F. Braun, and M. Pelizzone, Phys. Rev. B **27**, 2800 (1983).
[25] C.B. Vining and R.N. Shelton, Phys. Rev. B **28**, 2732 (1983).
[26] P.G. de Gennes, J. Phys. Radium **23**, 510 (1962).
[27] D.R. Noakes and G.K. Shenoy, Phys. Lett. **91A**, 35 (1982).
[28] In the tetragonal symmetry of $M_5Rh_4Ge_{10}$, the crystal field is characterized by five parameters. The limited experimental data prevents us from the independent determination of all the crystal-field parameters unambiguously. In order to keep the number of parameters to a minimum, we retained the fourth-order cubic terms and second-order axial distortion term only. Details of the crystal-field analysis will be published elsewhere. In the present work, $B_z(0)$ is $B_2(0)$.
[29] R. Mallik, E.V. Sampathkumaran, M. Strecker, and G. Wortmann, Europhys. Lett. **41**, 315 (1998).
[30] Chandan Mazumdar, K. Ghosh, R. Nagaragan, S. Ramakrishnan, B. D. Padalia, and L. C. Gupta, Phys. Rev. B **59**, 4215 (1999).
[31] H.J. Zeiger and G.W. Pratt, *Magnetic Interactions in Solids* (Clarendon, Oxford, 1973), p. 247.
[32] It is also possible that CFE's could lead to anisotropic *g* factors for the ground doublet state. Inelastic neutron-scattering data are essential to settle this issue.
[33] R.J. Birgeneau, M.T. Hutchings, J.M. Baker, and J.D. Riley, J. Appl. Phys. **40**, 1070 (1969).